(3+1)-dimensional superluminal spatiotemporal optical solitons and vortices at weak light level

Hui-jun Li, Yuan-po Wu, Chao Hang, and Guoxiang Huang

Phys. Rev. A **86**, 043829 — Published 22 October 2012

DOI: 10.1103/PhysRevA.86.043829

(3+1)-Dimensional Superluminal Spatiotemporal Optical Solitons and Vortices at Weak Light Level

Hui-jun Li[1,a], Yuan-po Wu[1], Chao Hang[2], and Guoxiang Huang[2,b]

[1]*Institute of Nonlinear Physics, Zhejiang Normal University, Jinhua, 321004 Zhejiang, China*

[2]*State Key Laboratory of Precision Spectroscopy and Department of Physics, East China Normal University, 200062 Shanghai, China*

(Dated: October 5, 2012)

Abstract

A scheme is proposed to produce (3+1)-dimensional superluminal spatiotemporal optical solitons and vortices in a coherent atomic system working in an active Raman gain regime. It is shown that the evolution of the envelope of a signal field obeys a modified (3+1)-dimensional nonlinear Schrödinger equation, which includes dispersion, diffraction, and Kerr nonlinearity. Various solutions of light bullets, light vortices, light-bullet trains, and light-vortex trains are presented, which display many interesting characters, including superlumianl propagating velocity and extremely low generating power. In addition, they can be easily manipulated in a controllable way. Stabilization of such high-dimensional superluminal light bullets and vortices can be realized using the trapping potential formed by an additional far-detuned laser field.

PACS numbers: 42.65.Tg, 05.45.Yv

[a] Corresponding author: hjli@zjnu.cn

[b] Corresponding author: gxhuang@phy.ecnu.edu.cn

I. INTRODUCTION

Stable high-dimensional spatiotemporal optical solitons, alias light bullets (LBs) [1], appearing as a result of the interplay between dispersion, diffraction and nonlinearity, are of great interest due to their rich nonlinear physics and important practical applications [2–18]. Up to now, most LBs are produced in passive optical media, in which far off resonance excitation schemes are adopted to avoid significant optical absorption. However, such schemes have some shortcomings. For example, they require very high generating power needed to obtain nonlinearity strong enough to balance diffraction and dispersion, they are hard to achieve an active control on light bullet property due to the lack of energy-level structure and selection rules, etc. As a result, the propagating velocity of the LBs obtained with such schemes is not far from c (the light speed in vacuum), and so on.

It is desirable to design new LB generation schemes that may overcome the above shortcomings. Active (i.e. on-resonance) optical media, in which light interacts with matter resonantly, can be used to achieve such aim. However, for on-resonance media there is usually a very large optical absorption. In recent years there have been great interest focused on the wave propagation in active atomic systems via electromagnetically induced transparency (EIT) [19]. Based on EIT, it has been shown that optical solitons [20–26] and LBs [27] with ultraslow propagating velocity can form in various active atomic systems.

However, the EIT scheme has drawbacks of large pulse spreading at room temperature and very long response time due to ultraslow propagation. Parallel to EIT study, optical pulse propagation using active Raman gain (ARG) scheme has also been received much attention in recent years [28–44]. In an ARG system a temporary population inversion is established prior to the arrival of signal field. The gain can lead to many interesting propagation phenomena such as abnormal propagation velocity of a signal field. There are ample experimental observations showing apparent *superluminal* propagation (i.e., apparent group velocity exceeds c, or even becomes negative [28–44]) of optical pulses in the systems where gain is a dominate feature.

In the present work, we propose a scheme to produce LBs and vortices in a lifetime-broadened four-level atomic system, which interact resonantly with three laser fields and working in an ARG regime. Due the quantum interference effect induced by a control field, the gain of the system can be largely suppressed. By using standard method of multiple-

scales we derive an envelope equation for the signal field, which includes dispersion, diffraction, and Kerr nonlinearity of the system. We present various solutions of LBs, light vortices, LB trains, and light-vortex trains, and find that they possess many interesting characters, including superlumianl propagating velocity and extremely low generating power. In addition, they can be easily manipulated in a controllable way. Stabilization of such high-dimensional superluminal light bullets and vortices can be achieved using the trapping potential formed by an additional far-detuned laser field. As far as we know such superluminal light bullets and vortices have never been reported in literature up to now.

The article is arranged as follows. Sec. II gives an introduction of the model under study. Sec. III presents a derivation of (3+1)-dimensional [(3+1)D] [45] nonlinear envelope equation of signal field using a method of multiple scales. Sec. IV discusses the formation, propagation and their stability of superluminal LBs and vortices. Lastly, the final section summarizes the main results obtained in this work.

II. MODEL

We consider a lifetime-broadened atomic system of N-type energy-level configuration, see Fig. 1(a). A strong continuous-wave (CW) pump (weak pulsed signal) field with center angular frequency ω_p (ω_s) and half Rabi frequency Ω_p (Ω_s) couples resonantly with states $|1\rangle$ and $|3\rangle$ ($|2\rangle$ and $|3\rangle$). States $|1\rangle$, $|2\rangle$, and $|3\rangle$ together with the pump and signal fields constitute a Λ-type three-level ARG core. A strong CW control field with center angular frequency ω_c and half Rabi frequency Ω_c coupling with levels $|3\rangle$ and $|4\rangle$ is used to suppress the gain of the signal field. The electric-field vector that resonantly interacting with atoms is given by $\mathbf{E} = \sum_{l=p,s,c} \mathbf{e}_l \mathcal{E}_l \exp\left[i(\mathbf{k}_l \cdot \mathbf{r} - \omega_l t)\right] + \text{c.c.}$, where $\mathbf{e}_l$ ($\mathbf{k}_l$) is polarization direction (wave vector) of lth field with envelope $\mathcal{E}_l$. In addition, a far-detuned standing-wave laser field $\mathbf{E}_{\text{Stark}}(\mathbf{r}, t) = \mathbf{e}_L \sqrt{2} E_0(x, y) \cos(\omega_L t)$ is added to the system, where $\mathbf{e}_L$, ω_L are unit polarization vector and angular frequency, respectively. Due to the existence of $\mathbf{E}_{\text{Stark}}(\mathbf{r}, t)$, a small but space-dependent Stark level shift $\Delta E_j = -\frac{1}{2}\alpha_j \left\langle \mathbf{E}^2_{\text{Stark}} \right\rangle_t = -\frac{1}{2}\alpha_j E_0^2(x, y)$ occurs, here α_j is the scalar polarizability of the level $|j\rangle$, $\langle \cdots \rangle$ denotes the time average in an oscillating cycle. As we shall see below, the space-dependent Stark level shift will contribute a trapping potential to the signal-field envelope. All four laser beams are assumed to propagate along the z axis [see Fig. 1(b)], and the pump and sinal fields have large detunings. The

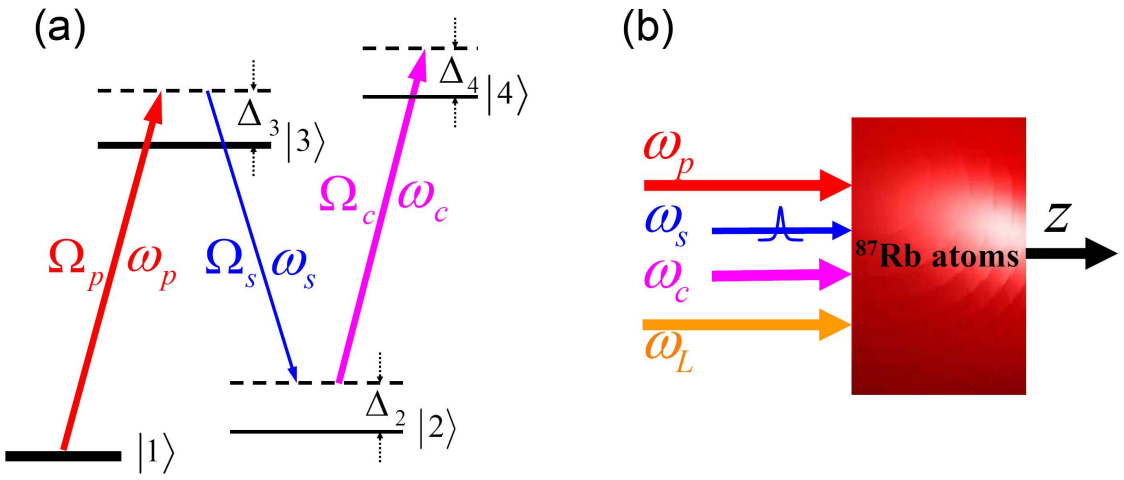

FIG. 1. (Color online) (a): Energy-level diagram and excitation scheme of the lifetime-broadened four-state atomic system interacting with a strong CW pump field (with half Rabi frequency Ω_p), a weak pulsed signal field (with half Rabi frequency Ω_s), a strong CW control field (with half Rabi frequency Ω_c). Δ_3, Δ_2, and Δ_4 are one-photon, two-photon, and three-photon detunings, respectively. (b): Possible arrangement of beam geometry. ω_p, ω_s, ω_c, ω_L are angular frequencies of the pump, signal, control, and far-detuned laser fields, respectively.

copropagating geometry and large detunings $\Delta_{3,4}$ chosen here are for suppressing the Doppler effect resulted from the thermal motion of atoms.

The Hamiltonian of the system in the interaction picture reads $\hat{H}_{\rm int} = -\hbar\sum_{j=1}^{4}[\Delta_j + \alpha_j E_0^2/(2\hbar)]|j\rangle\langle j| - \hbar(\Omega_p|3\rangle\langle 1| + \Omega_s|3\rangle\langle 2| + \Omega_c|4\rangle\langle 2| + \text{H.c.})$. Here $\Omega_p \equiv (\mathbf{e}_p \cdot \mathbf{p}_{13})\mathcal{E}_p/\hbar$, $\Omega_s \equiv (\mathbf{e}_s \cdot \mathbf{p}_{23})\mathcal{E}_s/\hbar$, $\Omega_c \equiv (\mathbf{e}_c \cdot \mathbf{p}_{24})\mathcal{E}_c/\hbar$, H.c. denotes Hermitian conjugate, and $\Delta_3 = \omega_p - (\omega_3 - \omega_1)$, $\Delta_2 = \omega_p - \omega_s - (\omega_2 - \omega_1)$, and $\Delta_4 = \omega_p - \omega_s + \omega_c - (\omega_4 - \omega_1)$ are the one-, two-, and three-photon detunings, respectively. The state vector of the system reads $|\Psi\rangle = \sum_{j=1}^{4} A_j \exp\{i[\mathbf{k}_j \cdot \mathbf{r} - (E_j/\hbar + \Delta_j)t]\}$, with E_j the bare state eigenenergy of the level $|j\rangle$, $\mathbf{k}_1 = 0$, $\mathbf{k}_2 = \mathbf{k}_p - \mathbf{k}_s$, $\mathbf{k}_3 = \mathbf{k}_p$, and $\mathbf{k}_4 = \mathbf{k}_p - \mathbf{k}_s + \mathbf{k}_c$. By Schrödinger equation $i\hbar\partial|\Psi\rangle/\partial t = \hat{H}_{\rm int}|\Psi\rangle$ one obtains the equations of motion on A_j $(j = 1, 2, 3, 4)$

$$\left(i\frac{\partial}{\partial t} + d_2\right) A_2 + \Omega_s^* A_3 + \Omega_c^* A_4 = 0, \tag{1a}$$

$$\left(i\frac{\partial}{\partial t} + d_3\right) A_3 + \Omega_p A_1 + \Omega_s A_2 = 0, \tag{1b}$$

$$\left(i\frac{\partial}{\partial t} + d_4\right) A_4 + \Omega_c A_2 = 0, \tag{1c}$$

with $\sum_{j=1}^{4}|A_j|^2=1$, where $d_j\equiv\Delta_j+\alpha_j E_0^2/(2\hbar)+i\gamma_j$ (j = 2-4), and γ_j is the decay rate of the state $|j\rangle$. The base state (i.e. the steady state of the system when the signal field is absent) is $A_1=1/\sqrt{1+|\Omega_p|^2/|d_3^{(0)}|^2}$, $A_2=A_4=0$, and $A_3=-(\Omega_p/d_3^{(0)})A_1$.

The electric-field evolution is governed by the Maxwell equation, which under a slowly varying envelope approximation is reduced to

$$i\left(\frac{\partial}{\partial z}+\frac{1}{c}\frac{\partial}{\partial t}\right)\Omega_s+\frac{c}{2\omega_s}\left(\frac{\partial^2}{\partial x^2}+\frac{\partial^2}{\partial y^2}\right)\Omega_s+\kappa_{23}A_3A_2^*=0, \tag{2}$$

where $\kappa_{23}=N\omega_s|\mathbf{e}_s\cdot\mathbf{p}_{23}|^2/(2\epsilon_0\hbar c)$, with N being the atomic concentration.

III. (3+1)D NONLINEAR ENVELOPE EQUATION

For studying the nonlinear evolution and the formation of possible LBs and vortices in the system, we employ the standard method of multiple-scales [46] to investigate the evolution of the signal field. We make the asymptotic expansion $A_j=\sum_{l=0}\epsilon^l A_j^{(l)}$, $\Omega_s=\sum_{l=0}\epsilon^l\Omega_s^{(l)}$, and $E_0=\epsilon E_0'$, here ϵ being a small parameter characterizing the typical amplitude of the signal field. To obtain divergence-free expansions, all quantities on the right hand sides of the asymptotic expansions are considered as functions of multi-scale variables $x_1=\epsilon x$, $y_1=\epsilon y$, $z_l=\epsilon^l z$ ($l=0,1,2$), and $t_l=\epsilon^l t$ ($l=0,1$). Substituting this expansion into Eqs. (1) and (2), one can obtain a series of linear but inhomogeneous equations for $A_j^{(l)}$ and $\Omega_s^{(l)}$, which can be solved order by order.

At the zero-order ($l=0$), one obtains $A_1^{(0)}=1/\sqrt{1+|\Omega_p|^2/|d_3^{(0)}|^2}$, $A_2^{(0)}=A_4^{(0)}=0$, and $A_3^{(0)}=-(\Omega_p/d_3^{(0)})A_1^{(0)}$. At the first-order ($l=1$), one get the linear solution, which reads

$$\Omega_s^{(1)}=F\,e^{i\theta}, \tag{3a}$$

$$A_2^{(1)}=-\frac{A_3^{(0)}}{D}(\omega-d_4^{(0)})F^*e^{-i\theta^*}, \tag{3b}$$

$$A_4^{(1)}=-\frac{\Omega_c A_3^{(0)}}{D}F^*e^{-i\theta^*}, \tag{3c}$$

and $A_1^{(1)}=A_3^{(1)}=0$. Here $D\equiv|\Omega_c|^2-(\omega-d_2^{(0)})(\omega-d_4^{(0)})$ (with $d_j^{(0)}\equiv\Delta_j+i\gamma_j$), F is yet to be determined envelope function depending on slow variables t_1, z_1, and z_2, $\theta\equiv K(\omega)z_0-\omega t_0$ [47] with the linear dispersion relation given by

$$K(\omega)=\frac{\omega}{c}-\frac{\kappa_{23}|A_3^{(0)}|^2}{D^*}\left(\omega-d_4^{*(0)}\right). \tag{4}$$

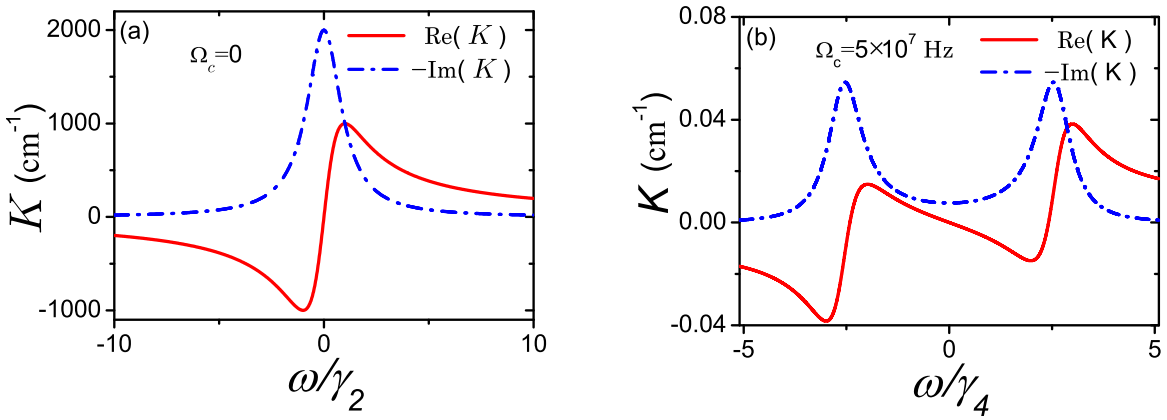

FIG. 2. (Color online) The linear dispersion relation K of the signal field as functions of dimensionless frequency $\omega/\gamma_{2,4}$. Panels (a) and (b) correspond to the absence ($\Omega_c = 0$) and the presence ($\Omega_c = 5 \times 10^7$ Hz) of the control field, respectively. In both panels, the solid and dashed-dotted lines denote respectively the real part $\mathrm{Re}(K)$ and the negative imaginary part $-\mathrm{Im}(K)$ of K.

Fig. 2 shows $K(\omega)$ as a function of dimensionless frequency $\omega/\gamma_{2,4}$. System parameters used are $\gamma_1 = \Delta_{2,4} = 0$, $2\gamma_2 = 1 \times 10^3\,\mathrm{Hz}$, $2\gamma_3 = 2\gamma_4 = 36\,\mathrm{MHz}$, $\kappa_{23} = 1.0 \times 10^{10}\,\mathrm{cm}^{-1}$ Hz, and $\Delta_3 = -2.0 \times 10^9$ Hz. Panels (a) and (b) correspond to the absence ($\Omega_c = 0$) and the presence ($\Omega_c = 5 \times 10^7$ Hz) of the control field, respectively. The solid and the dashed-dotted lines in both panels denote the real part $\mathrm{Re}(K)$ and the negative imaginary part $-\mathrm{Im}(K)$ of K, respectively. We see that when $\Omega_c = 0$, the signal field has a large gain [the dashed-dotted line in panel (a)]; however, a nearly gain-free window is opened when Ω_c is applied [the dashed-dotted line of panel (b)]. The suppression of the gain comes from the quantum interference effect induced by the control field. The steep slope for the large control field in the solid line of panel (b) gives a superluminal group velocity at the center frequency of the signal field (i.e. $\omega = 0$).

At the second-order ($l = 2$), the solvability condition for $A_j^{(2)}$ and $\Omega_s^{(2)}$ requires that in this order the envelope F travels with complex group velocity $V_g = (\partial K/\partial\omega)^{-1}$. At the third order ($l = 3$), the solvability condition requires

$$i\frac{\partial}{\partial z_2}F + \frac{c}{2\omega_s}\left(\frac{\partial^2}{\partial x_1^2} + \frac{\partial^2}{\partial y_1^2}\right)F - \frac{1}{2}K_2\frac{\partial^2 F}{\partial t_1^2} + \alpha_{11}|F|^2F + \alpha_{12}E_0'^2F = 0, \tag{5}$$

where $K_2 = \partial^2 K/\partial\omega^2$, and

$$\alpha_{11} = -\frac{\kappa_{23}}{D^*}(\omega - d_4^*)\left(A_3^{*(0)}a_3^{(2)} + A_3^{(0)}a_3^{*(2)}\right), \tag{6a}$$

$$\alpha_{12} = \frac{\kappa_{23}|A_3^{(0)}|^2}{2\hbar D^{*2}}\left[\alpha_2^*(\omega - d_4^{(0)*})^2 + \alpha_4^*|\Omega_c|^2\right], \tag{6b}$$

with

$$a_3^{(2)} = \frac{A_3^{(0)}}{d_3^{(0)}D}\left(\omega - d_4^{(0)}\right) - \frac{|A_3^{(0)}|^2 A_3^{(0)}}{2}\left[\frac{|\omega - d_4^{(0)}|^2 + |\Omega_c|^2}{|D|^2} + \frac{\omega - d_4^{(0)*}}{d_3^{(0)*}D^*} + \frac{\omega - d_4^{(0)}}{d_3^{(0)}D}\right].$$

Combining above results, we obtain

$$i\left(\frac{\partial}{\partial z} + \frac{1}{V_g}\frac{\partial}{\partial t}\right)U + \frac{c}{2\omega_s}\left(\frac{\partial^2}{\partial x^2} + \frac{\partial^2}{\partial y^2}\right)U - \frac{1}{2}K_2\frac{\partial^2 U}{\partial t^2} + \alpha_{11}|U|^2U + \alpha_{12}E_0^2U = 0, \tag{7}$$

after returning to the original variables, where $U \equiv \epsilon F$.

IV. SUPERLUMINAL LBS AND VORTICES, AND THEIR STABILITY

From Eq. (7) we see that the envelope of the signal field obeys a (3+1)D nonlinear Schrödinger (NLS) equation, which include dispersion, diffraction, Kerr nonlinearity. In addition, the last term on the left hand side of Eq. (7) is the one contributed from the far-detuned laser field, which can be used to stabilize (3+1)D nonlinear excitations in the system, as shown below.

A. Estimation of the coefficients in the nonlinear envelope equation

We now seek possible (3+1)D LBs and vortices based on Eq. (7). For convenience of following calculations, we convert them into the dimensionless form

$$i\frac{\partial u}{\partial s} + \frac{1}{2}\left(\frac{\partial^2}{\partial\xi^2} + \frac{\partial^2}{\partial\eta^2} + g_d\frac{\partial^2}{\partial\tau^2}\right)u + g_{11}|u|^2u + g_{12}V(\xi,\eta)u = 0, \tag{8}$$

with $u \equiv U/U_0$, $V(\xi,\eta) \equiv (E_0(\xi,\eta)/E_{10})^2$, $s \equiv z/L_{\rm diff}$, $\tau \equiv (t - z/{\rm Re}(V_g))/\tau_0$, $(\xi,\eta) \equiv (x,y)/R_\perp$, $g_d \equiv -L_{\rm diff}K_2/\tau_0^2$, $g_{11} \equiv \alpha_{11}/|\alpha_{11}|$, and $g_{12} \equiv \alpha_{12}E_{10}^2/|\alpha_{11}U_0^2|$. Here $L_{\rm diff} \equiv \omega_s R_\perp^2/c$ (with $R_\perp$ being typical beam radius) is typical diffraction length, and τ_0 is typical pulse length of the signal field. Note that we have taken $L_{\rm diff} = L_{NL}$ [with $L_{NL} = 1/(|\alpha_{11}U_0^2|)$ being a typical nonlinear length], thus $U_0 = \sqrt{c/(\omega_s R_\perp^2|\alpha_{11}|)}$ (typical Rabi frequency of the signal field). E_{10} is typical field intensity of the far-detuned laser field, which can be used

to adjust the magnitude of the trapping potential $V(\xi,\eta)$, and hence control the stability of the (3+1)D LBs and vortices.

Because the system under study is an active and lifetime-broadened one, the coefficients in Eq. (8) are generally complex. If the control-field half Rabi frequency Ω_c is small, the imaginary parts of the coefficients are comparable with their real parts, and hence stable nonlinear excitations do not exist. However, it is easy to show that under the ARG condition $|\Omega_c|^2 \gg \gamma_2\gamma_4$ the gain of the signal field can be largely suppressed due to the quantum interference effect induced by the control field, and thus the imaginary parts of these coefficients can be made to be much smaller than their real parts.

To show this we make an estimation on the value of the coefficients in Eq. (8). Consider a typical atomic gas of ^{87}Rb atoms, with D_1 line transitions $5^2S_{1/2} \to 5^2P_{1/2}$. The energy levels are chosen as those in Fig. 1(a), with the states selected as $|1\rangle = |5S_{1/2}, F = 1, m_F = -1\rangle$, $|2\rangle = |5S_{1/2}, F = 2, m_F = 0\rangle$, $|3\rangle = |5P_{1/2}, F = 2, m_F = -1\rangle$, $|4\rangle = |5P_{1/2}, F = 2, m_F = 1\rangle$. From the data of ^{87}Rb [48], we have $\mathbf{p}_{23} = -\sqrt{\frac{1}{4}} \times 2.54 \times 10^{-27}$ cm C. Other system parameters are given by $2\gamma_2 = 1 \times 10^3$ Hz, $2\gamma_{3,4} = 36$ MHz, $\kappa_{23} = 1.0 \times 10^{10}$ cm^{-1}Hz, $\omega_s = 2.37 \times 10^{15}$ Hz, $R_\perp = 3.7 \times 10^{-3}$ cm, $\Omega_c = 6.0 \times 10^7$ Hz, $\Omega_p = 5.0 \times 10^7$ Hz, and $\Delta_2 = 1.0 \times 10^4$ Hz. When these parameters are fixed, we have still other parameters Δ_3, Δ_4, τ_0, and E_{10} that can be chosen and adjusted in a fairly arbitrary domain. Thus we can obtain many different regimes, two of which are listed in the following:

Regime 1 (Self-focusing nonlinearity) : $\Delta_3 = -6.0 \times 10^8$ Hz, $\Delta_4 = -2.0 \times 10^9$ Hz, $\tau_0 = 5.0 \times 10^{-6}$ s, $E_{10} = 420$ V cm^{-1}. We have $L_{\rm diff} = 1.08$ cm, $U_0 = 2.49 \times 10^6$ Hz, $\mathrm{Re}(V_g)/c = -1.58 \times 10^{-6}$, and thus we have

$$g_d = 1.01 + 0.03i, \quad g_{11} = 1.0 + 0.01i, \quad g_{12} = 1.0 + 0.02i. \tag{9}$$

Regime 2 (Self-defocusing nonlinearity) : $\Delta_3 = 6.0 \times 10^8$ Hz, $\Delta_4 = -6.0 \times 10^8$ Hz, $\tau_0 = 8.3 \times 10^{-7}$ s, $E_{10} = 1383$ V cm^{-1}. We have $L_{\rm diff} = 1.08$ cm, $U_0 = 1.50 \times 10^7$ Hz, $\mathrm{Re}(V_g)/c = -1.73 \times 10^{-5}$, and hence one has

$$g_d = 1.01 + 0.09i, \quad g_{11} = -1.0 - 0.03i, \quad g_{12} = 1.0 + 0.06i. \tag{10}$$

We see that the imaginary parts of the coefficients in Eq. (8) are indeed much smaller than their corresponding real parts. The physical reason for so small imaginary parts is, as mentioned above, due to the quantum interference effect induced by the control field. In the

following discussion, the small imaginary parts of the coefficients are neglected for analytical analysis, but included in numerical simulations. We also see that due to the active character of the system, one can obtain the case of self-focusing where $g_{11} \approx 1$ (Regime 1) and the case of self-defocusing where $g_{11} \approx -1$ (Regime 2).

Equation (8) without the trapping potential (i.e., $g_{12} = 0$) is a (3+1)D NLS equation. In such case, even if a LB is excited initially, it will be unstable [2, 3]. Our aim is not only to obtain a (3+1)D LB, but also to provide a way to stabilize it. Thus in our model the far-detuned laser field has been added, which contributes a trapping potential to the signal field and hence can stabilize the LB formed by the signal field.

The far-detuned laser field is an "external" field, which can be selected very arbitrarily. Here we assume $E_0(x, y)$ is a Bessel beam, so that $V(\xi, \eta) = c_0^2 \left[J_l(\sqrt{2b}r)\right]^2$. Here c_0 is an arbitrary constant, $r = \sqrt{\xi^2 + \eta^2}$, and J_l being the lth-order Bessel function. Then Eq. (8) becomes

$$i\frac{\partial u}{\partial s} + \frac{1}{2}\left(\frac{\partial^2}{\partial \xi^2} + \frac{\partial^2}{\partial \eta^2} + \frac{\partial^2}{\partial \tau^2}\right) u + g_{11}|u|^2 u + g_{12} c_0^2 \left[J_l(\sqrt{2b}r)\right]^2 u = 0. \tag{11}$$

Using the further transformation $u = \psi \exp(i\mu s)$, Eq. (11) becomes

$$\left(\frac{\partial^2}{\partial \xi^2} + \frac{\partial^2}{\partial \eta^2} + \frac{\partial^2}{\partial \tau^2}\right) \psi - 2\mu\psi + 2g_{11}|\psi|^2\psi + 2c_0^2 g_{12} \left[J_l(\sqrt{2b}r)\right]^2 \psi = 0, \tag{12}$$

where ψ is an complex function and μ is the propagation constant.

Once a solution ψ of Eq. (12) is obtained, one can analyze its linear stability by considering a perturbation to it, i.e.

$$u(\xi, \eta, \tau, s) = [\psi + (w_1 + w_2)\exp(\lambda s) + (w_1^* - w_2^*)\exp(\lambda^* s)]\exp(i\mu s), \tag{13}$$

where $w_{1,2} = w_{1,2}(\xi, \eta, \tau)$ and λ are normal mode and the corresponding eigenvalue of the perturbation, respectively. Substituting Eq. (13) into Eq. (11), one obtains the linear eigenvalue problem

$$-i\lambda w_1 = \frac{1}{2}\left(\frac{\partial^2}{\partial \xi^2} + \frac{\partial^2}{\partial \eta^2} + \frac{\partial^2}{\partial \tau^2}\right) w_2 + L_0 w_1 + L_+ w_2, \tag{14a}$$

$$-i\lambda w_2 = \frac{1}{2}\left(\frac{\partial^2}{\partial \xi^2} + \frac{\partial^2}{\partial \eta^2} + \frac{\partial^2}{\partial \tau^2}\right) w_1 - L_0 w_2 + L_- w_1, \tag{14b}$$

with $L_0 = \frac{g_{11}}{2}\left(\psi^2 - \psi^{*2}\right)$, $L_\pm = -\mu + 2g_{11}|\psi|^2 + c_0^2 g_{12}\left[J_l(\sqrt{2b}r)\right]^2 \mp \frac{g_{11}}{2}\left(\psi^2 + \psi^{*2}\right)$, which can be solved numerically by using the method in Ref. [49]. The solution ψ is stable if the real parts of all eigenvalues are negative or zero.

B. Superluminal LBs and light vortices

We now present various nonlinear solutions of Eq. (12) for the case of self-focusing nonlinearity ($g_{11} = 1$, $g_{12} = 1$) and check their stability by using numerical simulations.

1. Superluminal LBs

We first consider possible LB solutions. When taking $l = 0$, the external trapping potential in Eq. (12) is proportional to $\left[J_0(\sqrt{2}r)\right]^2$, where $J_0(\sqrt{2}r)$ is the zero-order Bessel function ($b = 1$ is chosen without loss of generality). Fig. 3(a) and Fig. 3(b) give isosurfaces ($|\psi| = 0.01$) of two LB solutions for $(c_0, \mu) = (1.8, 1.4)$ and for $(c_0, \mu) = (2.3, 2.7)$, respectively. The LB solutions are obtained by numerically solving Eq. (12) based on the modified squared-operator method (see Ref. [49]). Initial trial functions in the numerical simulation are of Gaussian types, which evolve into the ground state of Eq. (12), i.e. the LB solutions of the system.

The stability of the LBs obtained can be checked by using the Vakhitov-Kolokolov (VK) criterion [50]. For this aim, we calculate the power of the signal field defined by $P = 2\pi \iiint_{-\infty}^{+\infty} |\psi|^2 d\xi d\eta d\tau$, which is a function of the propagation constant μ and the potential strength constant c_0, with the result shown in Fig. 3(c). According to the VK criterion, the domains where the LBs are stable are the ones with $dP/d\mu > 0$, which are clearly illustrated in the figure.

The stability of the LB solutions is also checked by numerically solving the eigenvalue problem (14). The Fourier collocation method combining the Newton conjugate gradient method introduced in Ref. [49] is used. The result of the real part of maximum eigenvalue [i.e. $\mathrm{Re}(\lambda)$] as a function of μ and c_0 is shown in Fig. 3(d). One sees that the stability domains of the LBs [i.e. the domains where $\mathrm{Re}(\lambda)$ is non-positive] are the same as those obtained by using the VK criterion, and the stability domains become larger for larger c_0. This is easy to understand because a larger c_0 means a stronger trapping of the LB provided by the external potential. Hence, one can adjust the far-detuned laser field, and hence the external potential, to control the existence domain of the LB, which is easy to realize physically in the present active system.

High-order LB solutions for $l \geq 1$ can also be obtained, and their stability domains can

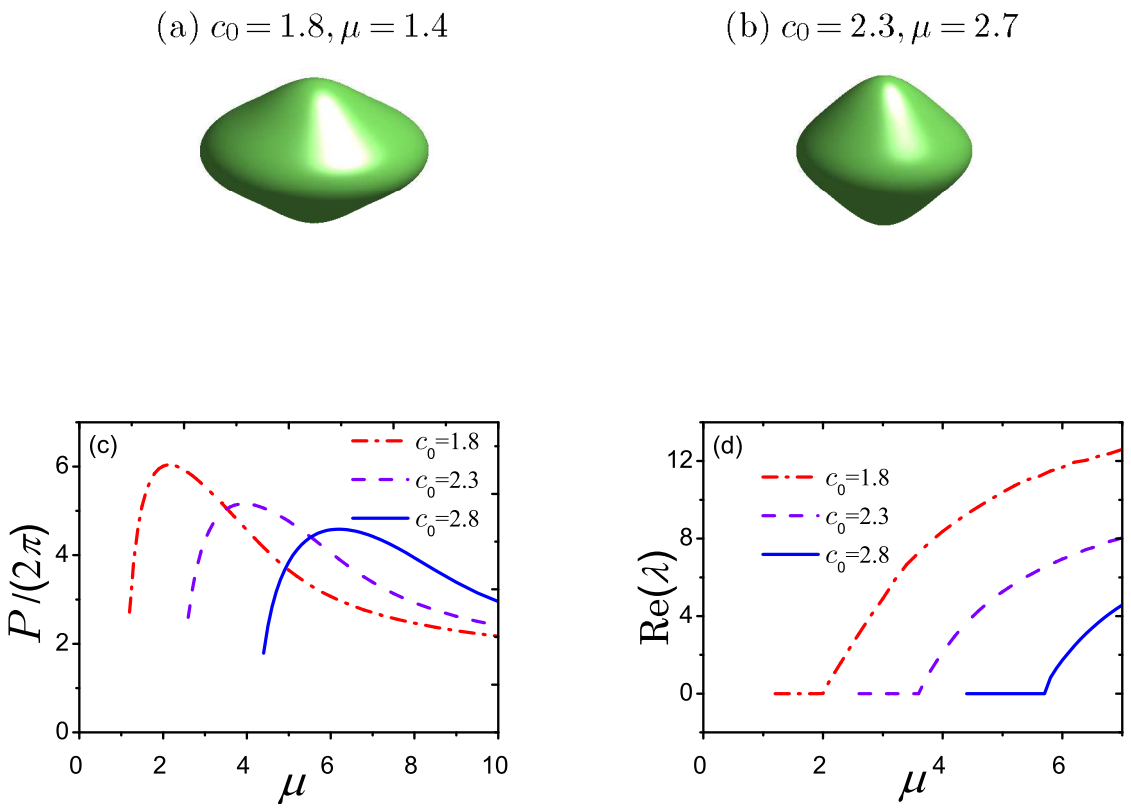

FIG. 3. (Color online) (a) and (b): Isosurface ($|\psi| = 0.01$) plots of LBs in the self-focusing case ($g_{11} = 1$, $g_{12} = 1$) for $(c_0, \mu) = (1.8, 1.4)$ and $(c_0, \mu) = (2.3, 2.7)$, respectively. The external trapping potential contributed by the far-detuned laser field is zero-order (i.e. $l = 0$) Bessel function. (c): Signal-field power P as a function of μ and c_0. (d): The real part of maximum eigenvalue (i.e. Re(λ)) as a function of μ and c_0 obtained by solving the eigenvalue problem (14). In panels (c) and (d), the dotted-dashed, dashed, and solid lines are for $c_0 = 1.8, 2.3$, and 2.8, respectively.

also be identified in the similar way. Generally, the stability domains of the high-order LBs become narrower for increasing l because the strength of the trapping potential with the form $\left[J_l(\sqrt{2}r)\right]^2$ becomes weaker as l increases.

The LB solutions obtained are the stationary solutions of Eq. (11). Because $\tau = (t - z/\mathrm{Re}(V_g))/\tau_0$, we obtain the propagating velocity of the LBs given by $V_{\mathrm{LB}} = \mathrm{Re}(V_g)$, which is around $-1.58 \times 10^{-6}\, c$ based on the chosen parameters. Fig. 4 shows the evolution of dimensionless signal-field amplitude $|u(x = 0, y = 0, z, t/\tau_0)|$ as a function of dimensionless time t/τ_0 by numerically solving Eq. (11). One sees that the LB profile at $z = 0.5$ cm has an advancement comparing with the LB profile at $z = 0$. Thus the LB obtained displays

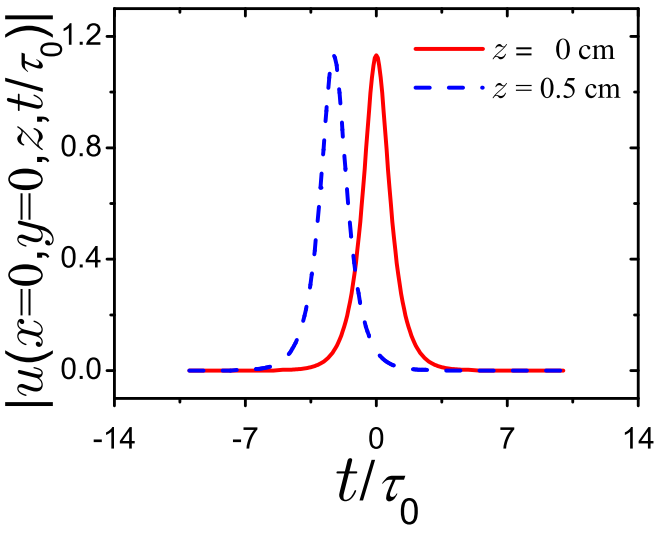

FIG. 4. (Color online) Evolution of $|u(x = 0, y = 0, z, t/\tau_0)|$ as a function of t/τ_0 and z by numerically solving Eq. (11). Solid red line and dashed blue line are for $z = 0$ and $z = 0.5$ cm, respectively.

indeed a superluminal propagation.

The peak power of the signal field may be estimated by calculating Poynting's vector, which is given by $\bar{P}_{\max} = 2\epsilon_0 c n_s S_0(\hbar/|\mathbf{p}_{23}|)^2 U_0^2 |u_{\max}|^2$, where n_s, S_0 and $u_{\max}$ are the reflective index, cross-section area of the signal beam, and the maximum of u, respectively. Taking $S_0 = \pi R_\perp^2 \approx 4.3 \times 10^{-5}$ cm^2 and using the other parameters given above, we obtain the generation power of the optical bullet given in Fig. 3(a) as $\bar{P}_{\max} \approx 0.01$ μ W. Consequently, the (3+1)D LBs obtained in the present active system have not only superluminal propagating velocity but also extremely low generation power.

2. *Superluminal light vortices*

We now turn to consider the case that the system allows (3+1)D light vortices, which are obtained by solving Eq. (12) numerically. Shown in Fig. 5 is the result for the zero-order ($l = 0$) light vortex. A isosurface plot with $|\psi| = 0.01$ for $(c_0, \mu) = (2.5, 0.9)$ and a 3D shaded surface plot of amplitude $|\psi|$ (i.e. $\tau = 0$) are shown in Fig. 5(a) and 5(b), respectively. The solution is obtained by using the modified squared-operator method [49]. The initial trial function is chosen as $\psi = A_0[r^2 + \tau^2]^{1/2} \mathrm{sech}(\sqrt{r^2 + \tau^2}) \exp(i\theta_1)$ with A_0 is the initial trial amplitude and (r, θ_1, τ) is the corresponding cylindrical coordinate system of (ξ, η, τ), which evolves into a light vortex.

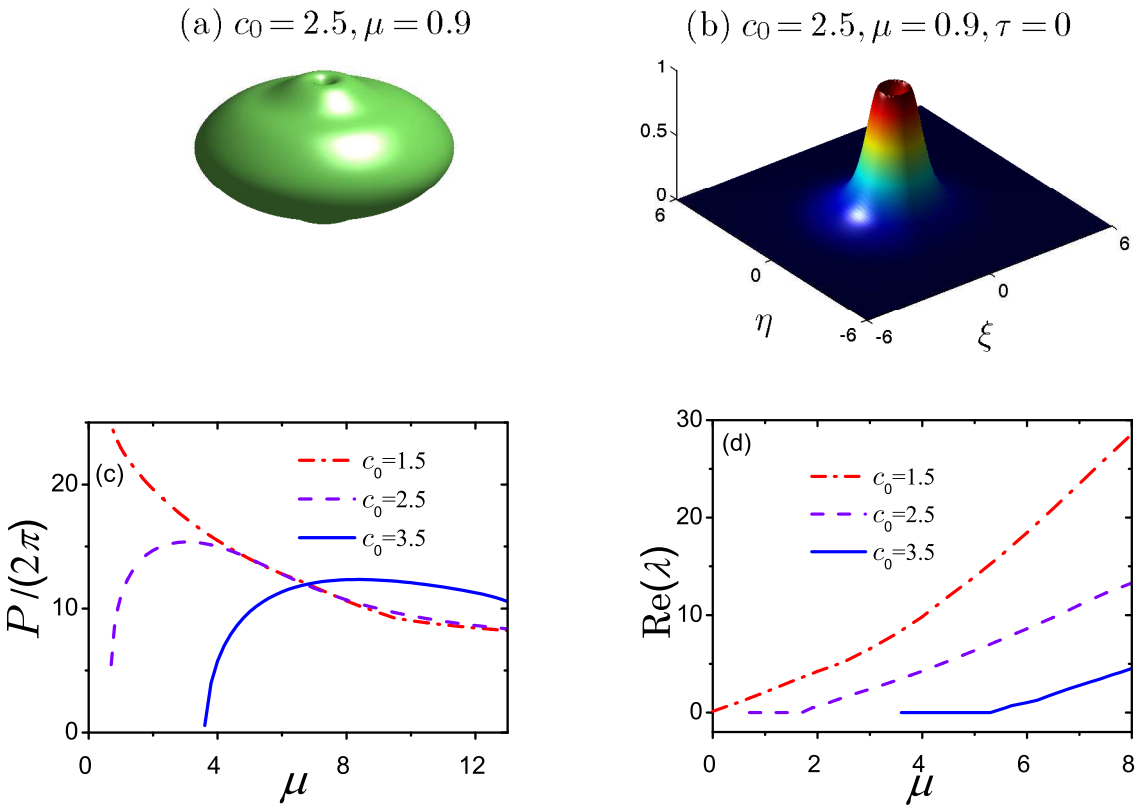

FIG. 5. (Color online) Isosurface plot (panel (a)) with $|\psi| = 0.01$ and 3D shaded surface (i.e. $\tau = 0$) plot (panel (b)) in the self-focusing case (i.e. $g_{11} = 1$, $g_{12} = 1$) for $(c_0, \mu) = (2.5, 0.9)$. The trapping potential contributed by the far-detuned laser field is zero-order (i.e. $l = 0$) Bessel function. (c): Signal-field power P as a function of μ and c_0. (d): Real part of maximum eigenvalue, i.e., Re(λ), as a function of μ and c_0 obtained by solving the eigenvalue problem (14). In panels (c) and (d), the dotted-dashed, dashed, and solid lines are for $c_0 = 1.5, 2.5$, and 3.5, respectively.

The power P of the signal field in the case of the light vortex as a function of μ and c_0 is shown in Fig. 5(c). The dotted-dashed, dashed, and solid lines in the figure are for $c_0 = 1.5, 2.5$, and 3.5, respectively. We see that P changes for different c_0. Note that although for vortices the VK criterion cannot apply, P curves of vortices can be taken to illustrate the existence domain of vortices. Interestingly, we find that for the present system the light vortex is stable in the domains where $dP/d\mu > 0$. Such conclusion is verified by a linear stability analysis of the light vortex by calculating maximum eigenvalue Re(λ) based on Eq. (14). The light vortex is stable in the domains where Re(λ) is zero or negative.

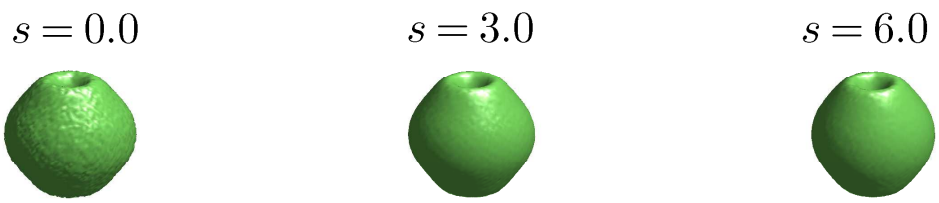

FIG. 6. (Color online) Isosurface plots for the evolution of a light vortex with $|u| = 0.1$ for $s = 0.0$, 3.0, and 6.0, respectively. The initial condition is taken as that given in Fig. 5(a).

Such domains are illustrated in Fig. 5(d), which coincide nearly with the domains where $dP/d\mu > 0$ in Fig. 5(c).

In the same way, the high-order light vortices for $l \geq 1$ can also be obtained, and their stability domains can also be identified. The existing and stability domains of the high-order light vortices are narrower because the strength of the trapping potential with the form $\left[J_l(\sqrt{2r})\right]^2$ becomes weaker as l increases.

The results presented above are the stationary solutions based on Eq. (12). It is necessary to consider the evolution and stability of the light vortices starting directly from Eq. (11) with complex coefficients. To this end, we make a numerical simulation on Eq. (11) by taking the light vortex solution obtained above as an initial condition, and add a random perturbation to it, i.e. we take $u(s = 0, \xi, \eta, \tau) = \psi(\xi, \eta, \tau)(1 + \varepsilon f)$. Here ε is a typical amplitude of the perturbation, and f is a random variable uniformly distributed in the interval $[0, 1]$. We find that Eq. (11) possesses indeed vortex solution that is fairly stable for propagating to a long distance. Shown in Fig. 6 is the evolution of a light vortex based on Eq. (11) by taking $\varepsilon = 0.1$ and the solution given in Fig. 5(a) as an initial condition. Illustrated are isosurface plots of the vortex with $|u| = 0.1$ for s=0.0, 3.0, and 6.0, respectively. We see the vortex is quite close to the initial unperturbed one after propagating $z = 6.48$ cm. The propagating velocity and generation power of the light vortex are $-1.58 \times 10^{-6}\, c$ and 0.01 μW, respectively.

C. Superluminal LB trains and light-vortex trains

Though in the case of self-defocusing nonlinearity (i.e., $g_{11} = -1$, $g_{12} = 1$) LBs and light vortices do not exist, the system however may support a LB-train and light-vortex train solutions, as shown below.

1. Superluminal LB trains

Shown in Fig. 7(a) is an isosurface plot with $|\psi| = 0.1$ for $(c_0, \mu) = (3, 2)$, $\tau = -3.8$ to 3.8, and $l = 0$. The solution is obtained by numerically solving Eq. (12) with $g_{11} = -1$ and $g_{12} = 1$. One sees that for such solution (called the zero-order LB train) light intensity distributes with the form of a train of round flat "cakes" along vertical (i.e. τ) direction.

Note that the similar LB train has also been obtained in Ref. [17]. However, formation reason of the structure is very different. In Ref. [17], the LB train is in fact a type of gap soliton induced by an external potential that consists of a transverse harmonic-oscillator potential and an axial periodic potential. Differently, in our model there is only a transverse Bessel potential. The reason for the appearance of periodic distribution in τ-direction is the following. The diffraction is balanced by the transverse Bessel potential and the self-defocusing Kerr nonlinearity. The competition between the dispersion term and linear term (i.e. $-2\mu\psi$) results in the formation of periodic distribution in τ-direction.

Shown in Fig. 7(b) is the power curve of the LB train as a function of μ and c_0, which illustrate the existence domain of the LB train. The solid, dashed, and solid-dashed lines are for $c_0 = 2.3, 2.6$, and 3.0, respectively. One sees that the existence domain of the LB train is increased when c_0 increases. The stability of the LB train is studied by solving the eigenvalue problem (14), with the result given in Fig. 7(c). One sees that the stability domain (i.e. the domain where $\mathrm{Re}(\lambda) \leq 0$) of the LB train coincides nearly with the existence domain. Similarly, high-order LB trains (i.e. $l \geq 1$) are also obtained, which are not presented here for saving space.

The time evolution of the LB train is investigated by taking the LB train solution given in Fig. 7(a) as an initial condition, with a random perturbation to it. Illustrated in Fig. 8 are respectively the isosurface plots for the evolution of the LB train based on Eq. (11) for $s = 0, 1.5$, and 4.5. We see that the LB train is indeed quite stable during propagation

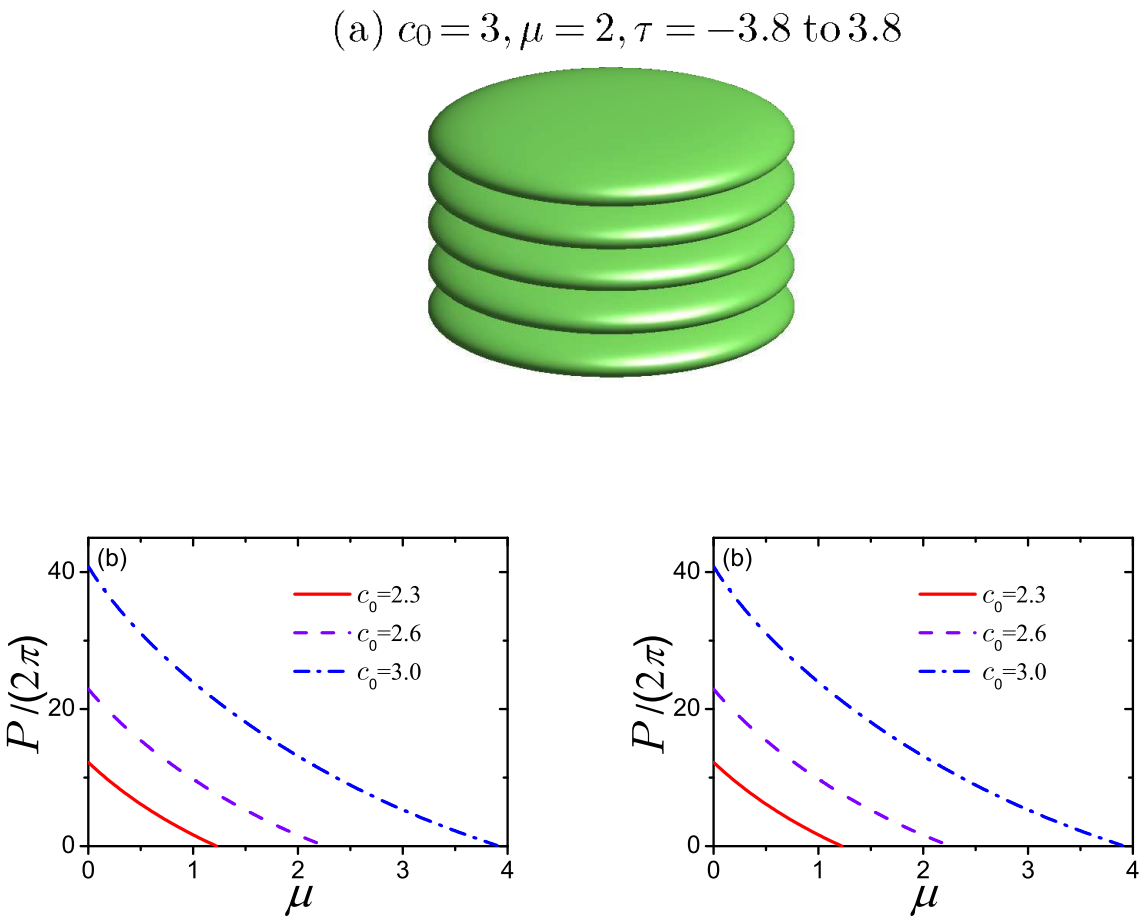

FIG. 7. (Color online) (a): Isosurface plot of the zero-order LB train with $|\psi| = 0.1$ in the self-defocusing case (i.e., $g_{11} = -1$, $g_{12} = 1$) for $(c_0, \mu) = (3, 2)$. (b): Signal-field power P as a function of μ and c_0. (c): Real part of maximum eigenvalue, i.e., Re(λ), as a function of μ and c_0 obtained by solving the eigenvalue problem (14). In panels (c) and (d), the solid, dashed, and dotted-dashed lines are for $c_0 = 2.3, 2.6$, and 3.0, respectively.

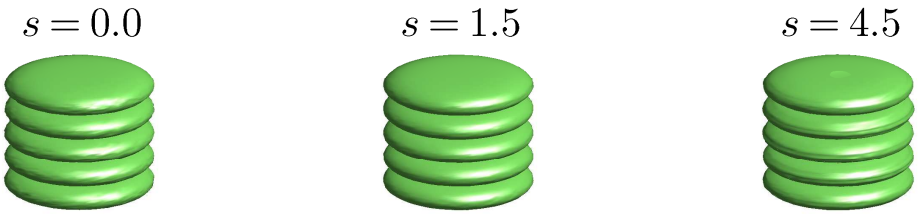

FIG. 8. (Color online) Isosurface plots for the evolution of the LB train with $|u| = 0.1$ for s=0.0, 3.0, 6.0 based on the results by solving Eq. (11). The initial condition is taken as that given in Fig. 7(a).

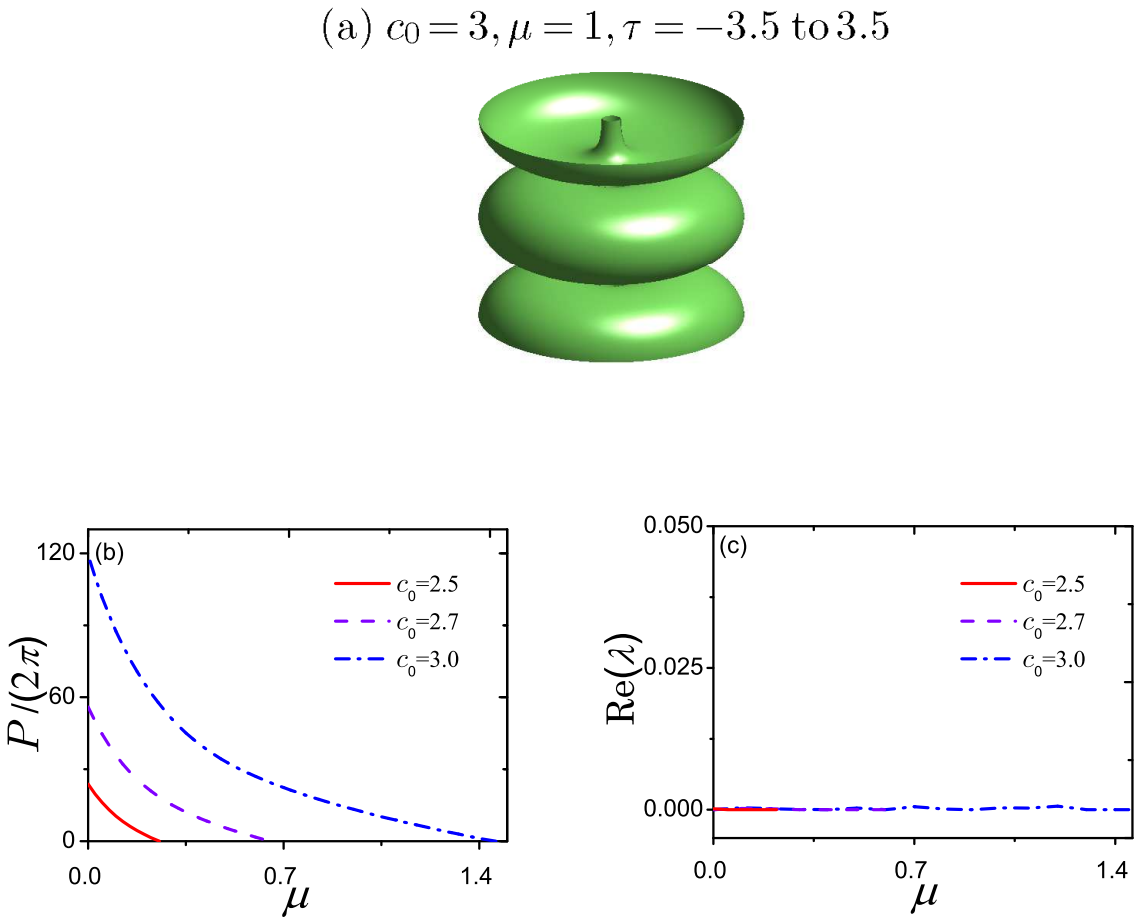

FIG. 9. (Color online) (a): Isosurface plot of the zero-order ($l = 0$) light-vortex train with $|\psi| = 0.3$ in the self-defocusing case (i.e., $g_{11} = -1$, $g_{12} = 1$) for $(c_0, \mu) = (3, 1)$, and τ from -3.5 to 3.5. (b): Signal-field power P as a function of μ and c_0. (c): Real part of maximum eigenvalue, i.e., Re(λ), as a function of μ and c_0 obtained by solving the eigenvalue problem (14). In panels (c) and (d), the solid, dashed, and dotted-dashed lines are for $c_0 = 2.5, 2.7$, and 3.0, respectively.

to a long distance. The propagating velocity and generation power of the LB train are $-1.73 \times 10^{-5}\, c$ and 0.86 μW, respectively.

2. *Superluminal light-vortex trains*

We finally present the result on the superluminal light-vortex trains in the system. Shown in Fig. 9 is the result for a zero-order (i.e. $l = 0$) light-vortex train. An isosurface plot of $|\psi| = 0.3$ for $(c_0, \mu) = (3, 1)$, and τ from -3.5 to 3.5 is shown in Fig. 9(a). The solution is

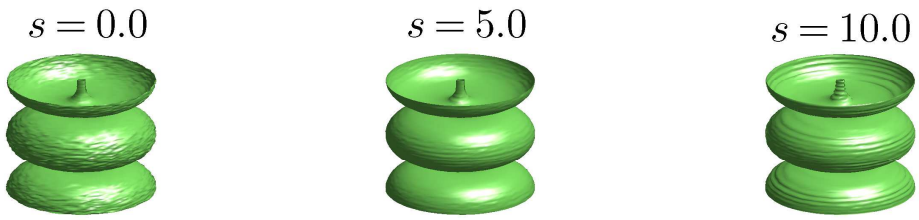

FIG. 10. (Color online) Isosurface plots for the evolution of the light-vortex train with $|u| = 0.3$ for s=0.0, 5.0, 10.0 based on solving Eq. (11). The initial condition is taken as that given in Fig. 9(a).

obtained by numerically solving Eq. (12) in terms of the modified squared-operator method [49].

The power curve P of the light-vortex train and the real part of maximum eigenvalue Re(λ) (based on solving Eq. (14)) as a functions of μ and c_0 have been presented respectively in Fig. 9(b) and Fig. 9(c). The solid, dashed, and dotted-dashed lines in both panels are for $c_0 = 2.5, 2.7$, and 3.0, respectively. The result shows that not only the light-vortex train exist, but also its existence domain and stability domain nearly coincide each other.

We have also investigated the evolution of the light-vortex train by numerically solving Eq. (11) and taking the solution given in Fig. 9(a) as an initial condition. Shown in Fig. 10 are the results for $s = 0.0, 5.0, 10.0$, respectively. To test its stability, a small random perturbation has been added in the calculation. We see that the light-vortex train is indeed stable during propagation to a long distance. The propagating velocity and generation power of the light-vortex train are $-1.73 \times 10^{-5}\, c$ and 0.32 μW, respectively. Thus, the light-vortex train obtained is a superluminal one and can be produced with extremely low generation power.

V. SUMMARY

In this article, we have proposed a scheme to produce (3+1)D superluminal light bullets and vortices in a coherent four-level atomic system interacting resonantly with three laser fields and working in ARG regime. We have proved that that the evolution of the envelope of the signal field satisfies a modified (3+1)D NLS equation, which includes dispersion, diffraction, and Kerr nonlinearity. Various solutions of light bullets, light vortices,

light-bullet trains, and light-vortex trains have been provided, which have many interesting features, including superlumianl propagating velocity and extremely low generating power, etc. Furthermore, they can be easily manipulated in a controllable way due to the active character of the system. In addition, we have demonstrated that the stabilization of such high-D superluminal localized optical structures can be realized using the trapping potential induced by an additional far-detuned laser field. The results presented here may be useful for understanding the physical properties of coherent atomic systems and guiding experimental findings of (3+1)D nonlinear excitations with very low generation power, which may have potential applications in optical information processing and transmission.

ACKNOWLEDGMENTS

Authors thank Jianke Yang for helpful discussions. This work was supported by the NSF-China under Grant Nos. 11105052, 11174080 and 11175158, by the NSF-Zhejiang province of China under Grant No. Y6100355, and by the Doctoral Foundation of ZJNU 2009.

[1] Y. Silberberg, Opt. Lett. **22**, 1282 (1990).

[2] B. A. Malomed, D. Mihalache, F. Wise, and L. Torner, J. Phys. B: Quantum Semiclass. Opt. **7**, R53 (2005), and references therein.

[3] Y. S. Kivshar and G. P. Agrawal, *Optical Solitons: From Fibers to Photonic Crystals* (Academic Press, London, 2006), and references therein.

[4] X. Liu, L. J. Qian and F. W. Wise, Phys. Rev. Lett. **82**, 4631 (1999).

[5] M. Blaauboer, B. A. Malomed, and G. Kurizki, Phys. Rev. Lett. **84**, 1906 (2000).

[6] I. N. Towers, B. A. Malomed, and F. W. Wise, Phys. Rev. Lett. **90**, 123902 (2003).

[7] P. Di Trapani, G. Valiulis, A. Piskarskas, O. Jedrkiewicz, J. Trull, C. Conti, and S. Trillo, Phys. Rev. Lett. **91**, 093904 (2003).

[8] D. Mihalache, D. Mazilu, F. Lederer, B. A. Malomed, Y. V. Kartashov, L.-C. Crasovan, and L. Torner, Phys. Rev. Lett. **95**, 023902 (2005).

[9] M. Matuszewski, E. Infeld, B. A. Malomed, and M. Trippenbach, Phys. Rev. Lett. **95**, 050403 (2005).

[10] L. Bergé and S. Skupin, Phys. Rev. Lett. **100**, 113902 (2008).

[11] M. Belić, N. Petrović, W. P. Zhong, R. H. Xie, and G. Chen, Phys. Rev. Lett. **101**, 123904 (2008).

[12] I. B. Burgess, M. Peccianti, G. Assanto, and R. Morandotti, Phys. Rev. Lett. **102**, 203903 (2009).

[13] S. H. Chen and J. M. Dudley, Phys. Rev. Lett. **102**, 233903 (2009).

[14] D. Abdollahpour, S. Suntsov, D. G. Papazoglou, and S. Tzortzakis, Phys. Rev. Lett. **105**, 253901 (2010).

[15] S. Minardi, F. Eilenberger, Y. V. Kartashov, A. Szameit, U. Röpke, J. Kobelke, K. Schuster, H. Bartelt, S. Nolte, L. Torner, F. Lederer, A. Tünnermann, and T. Pertsch, Phys. Rev. Lett. **105**, 263901 (2010).

[16] A. Muñoz Mateo, V. Delgado, and B. A. Malomed, Phys. Rev. A **82**, 053606 (2010).

[17] A. M. Mateo, V. Delgado, and B. A. Malomed, Phys. Rev. A **82**, 053606 (2010).

[18] D. Mihalache, J. Opt. Adv. Mat. **12**, 12 (2010).

[19] M. Fleischhauer, A. Imamoglu, and J. P. Marangos, Rev. Mod. Phys. **77**, 633 (2005), and references therein.

[20] Y. Wu and L. Deng, Phys. Rev. Lett. **93**, 143904 (2004).

[21] G. Huang, L. Deng and M. G. Payne, Phys. Rev. E. **72**, 016617 (2005).

[22] C. Hang and G. Huang, Phys. Rev. A **77**, 033830 (2008).

[23] W.-X. Yang, A.-X. Chen, L.-G. Si, K. Jiang, X. Yang, and R.-K. Lee, Phys. Rev. A **81**, 023814 (2010).

[24] T. Hong, Phys. Rev. Lett. **90**, 183901 (2003).

[25] H. Michinel, M. J. Paz-Alonso, and V. M. Perez-Garcia, Phys. Rev. Lett. **96**, 023903 (2006).

[26] C. Hang, V. V. Konotop, and G. Huang, Phys. Rev. A **79**, 033826 (2009).

[27] H. J. Li, Y. P. Wu, and G. Huang, Phys. Rev. A **84**, 033816(2011).

[28] R. Y. Chiao, Phys. Rev. A **48**, 34(R) (1993).

[29] R. Y. Chiao and A. M. Steinberg, in *Progress in Optics*, edited by E. Wolf (Elsevier, Amsterdam, 1997), p. 345.

[30] L. J. Wang, A. Kuzmich, and A. Dogariu, Nature (London) **406**, 277 (2000).

[31] A. Kuzmich, A. Dogariu, L. J. Wang, P. W. Milonni, and R. Y. Chiao, Phys. Rev. Lett. **86**, 3925 (2001).

[32] A. M. Akulshin, A. Cimmino, A. I. Sidorov, P. Hannaford, and G. I. Opat, Phys. Rev. A **67**, 011801(R) (2003).

[33] A. Lezama, A. M. Akulshin, A. I. Sidorov, and P. Hannaford, Phys. Rev. A **73**, 033806 (2006).

[34] M. S. Bigelow, N. N. Lepeshkin, and R. W. Boyd, Science **301**, 200 (2003).

[35] M. D. Stenner, D. J. Gauthier, and M. A. Neifield, Nature **425**, 695 (2003).

[36] R. G. Ghulghazaryan and Y. P. Malakyan, Phys. Rev. A **67**, 063806 (2003).

[37] K. Kim, H. S. Moon, C. Lee, S. K. Kim, and J. B. Kim, Phys. Rev. A **68**, 013810 (2003).

[38] L.-G. Wang, N.-H. Liu, Q. Ling, and S.-Y. Zhu, Phys. Rev. E **68**, 066606 (2003).

[39] E. E. Mikhailov, V. A. Sautenkov, I. Novikova, and G. R. Welch, Phys. Rev. A **69**, 063808 (2004).

[40] M. Janowicz and J. Mosttowski, Phys. Rev. E **73**, 046613 (2006).

[41] K. J. Jiang, L. Deng, and M. G. Payne, Phys. Rev. A **74**, 041803(R) (2006).

[42] J. Zhang, G. Hernandez, and Y. Zhu, Opt. Lett. **31**, 2598 (2006).

[43] P. W. Milonni, *Fast Light, Slow Light and Left-Handed Light* (Institute of Physics Publishing, Bristol and Philadelphia, 2005), and references therein.

[44] A. M. Akulshin, R. J. McLean, J. Opt. **12**, 104001 (2010).

[45] Here '3' denotes two transverse dimensions and one temporal dimension, and '1' denotes one spatial dimension in propagating direction.

[46] A. Jeffery and T. Kawahara, *Asymptotic Methods in Nonlinear Wave Theory* (Pitman, London, 1982).

[47] The frequency and wave vector of the signal field are given by $\omega_s+\omega$ and $k_s+K(\omega)$, respectively. Thus $\omega = 0$ corresponds to the center frequency of the signal field.

[48] D. A. Steck, Rubidium 87 D Line Data, http://steck.us/alkalidata/.

[49] J. Yang, *Nonlinear Waves in Integrable and Nonintegrable Systems* (SIAM, Philadelphia, 2011).

[50] M. G. Vakhitov and A. A. Kolokolov, Sov. J. Radiophys. Quantum Electron. **16**, 783 (1973).